Journal of Low Temperature Physics

Optomechanical Design for Optical Performance Characterization of W-band Kinetic Inductance Detectors

D. Arrazola[1] · M. C. de Ory[2,3] · B. Aja[4] · L. de la Fuente[4] · J. P. Pascual[4] · E. Artal[4] · D. Granados[3] · A. Gomez[2]

Abstract
A millimeter wave quasi-optical system is specially designed for the optical cryogenic characterization of superconducting kinetic inductance detectors for the W-band. The system includes a horn antenna optimized for the W-band, the optical instrument that comprises a collimator and collector subsystems and a set of thermal and microwave blocking filters. The completed design is described based on the Gaussian beam and ray tracing approximation. The accuracy of the Gaussian beam approximation is used to avoid losses by vignetting and to optimize *f*/0.9 collector optics at 92.5 GHz. The final opto-mechanical design is showed.

Keywords KIDs · Optical design · W-band · Gaussian method

1 Introduction

Kinetic inductance detectors (KIDs) have emerged as the new generation of millimeter wave superconducting detector for future astronomical experiments where large format cameras are needed [1]. With the aim of characterizing KIDs optical performance, a specific cryogenic quasi-optical set-up is required [2, 3]. A cryogenic opto-mechanical design working in the W-band is presented where, due to the diffraction

✉ D. Arrazola
david.arrazola@uah.es

✉ A. Gomez
agomez@cab.inta-csic.es

[1] Dpt. Physics and Mathematics, University of Alcalá, 28805 Alcalá de Henares, Spain

[2] Centro de Astrobiología (CSIC-INTA), Ctra. Torrejón-Ajalvir km. 4, 28850 Torrejón de Ardoz, Madrid, Spain

[3] IMDEA-Nanociencia, 28049 Cantoblanco, Madrid, Spain

[4] Dpt. Ing. Comunicaciones, University of Cantabria, 39005 Santander, Spain

limit, both ray tracing and Gaussian beam propagation has been performed [4]. The main requirements related to the detector have been the coupling efficiency and telecentricity, whereas the Point Spread Function (PSF) and Encircled Energy (EE) are the merit functions used in the optimization step. This system will be installed in order to characterize under incident wave illumination the developed LEKIDs optimized for the W-band explained elsewhere [5].

2 Optical Set-Up

Figure 1 shows an overview of the developed refractive optical testbed. It is a refractive instrument optimized at 92.5 GHz with diffraction limited performance. The following constrictions have been considered as starting points:

- *Mechanical constrictions* The cryostat dimensions are limitations for the design. First, the cryostat window with a diameter of 50 mm fixes the collimator which is adapted to minimize energy losses. Also, the available space inside the cryostat and cooling power limits the cold optics distance (~ 160 mm) and the number of cold elements (Fig. 1).
- *Optical constraints* Diffraction limited system, telecentricity, vignetting, coupling efficiency should be optimized for the detector dimensions (focal plane of 10×10 mm^2, pixel size 3×3 mm^2 and pitch between pixels 3.4 mm). Also, due to the working frequency band and cryogenic conditions, all lenses are made of High-Density Polyethylene (HDPE), which has an index refraction of 1.48 and negligible attenuation loss in the W-band.
- *Straylight and spurious radiation* A pupil stop is added in the collimated region at room temperature and a field stop in collector part at cryogenic temperatures are included for its minimization [2, 3].

The main parts of the testbed developed are described in next sections.

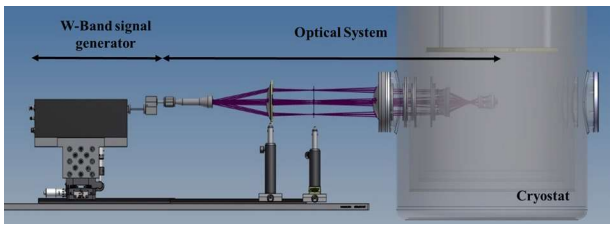

Fig. 1 Complete optical set-up showing the collimator optics at room temperature (left) and cryogenic set-up (right) (Color figure online)

2.1 Generation of W-band Signal

The millimeter band signal is generated using a microwave signal generator followed by a multiplier. Then, it is focused on the system using a horn antenna specially designed for the W-band; the rectangular feedhorn aperture dimensions are 14.8×11.0 mm^2 and the 3 dB beamwidth is 17°. It is worth noting that it is necessary to guarantee that the next optical element (collimator) is sufficiently far from the horn antenna (Fraunhofer distance L) which is calculated following Eq. (1) being D the feedhorn width and $\lambda_{\min}$ the minimum wavelength. In our case, we have set this distance to 100 mm.

$$L = \frac{D^2}{\lambda_{\min}} = 80.2\,\text{mm} \quad \begin{cases} D = 14.8\,\text{mm} \\ \lambda_{\min} = 2.73\,\text{mm}\,(110\,\text{GHz}) \end{cases} \tag{1}$$

2.2 Collimator Optical Design

The collimator is in the room temperature stage (red part in Fig. 2). As shown in Fig. 2, it includes 2 lenses, one collimator lens ($L1$) and a second lens ($L2$) in front of the external cryostat window to reduce energy losses. The lenses thickness has been limited in order to avoid high absorption of the signal that increases the noise contribution. Relevant parameters as radius, conic constant, thickness, and semi-diameter of each surface are included. To avoid spurious light, a pupil stop of 38 mm diameter is located between both lenses.

The effect of the cryostat window aperture limitation has been analyzed using the Gaussian propagation tool. The beam waist radius is the solution of the paraxial

Collimator Optics*				
	Radius	k	Thickness	Semi Aperture
L1	74,21	-	13,97	35,5
	Infinity	-		35,3
L2	54,65	-	12,76	37,9
	31,35	-2,98		34,5

Collector Optics*				
	Radius	k	Thickness	Semi Aperture
L3	25,57	-0,687	23,05	29,8
	79,07			24,2
L4	-49,69		10,35	11
	-19,61	0,913		12
L5	6,42	-0,975	22,65	13,4
	-57,15			13

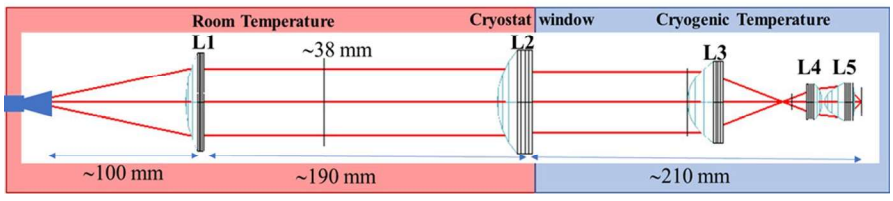

Fig. 2 Millimeter wave optical design including collimator and collector optics and relevant parameters. Filters are not shown for clarity. *Dimensions are shown in mm (Color figure online)

wave equation, and it is fixed with the feedhorn parameters. As the beam propagates, it spreads out, and its on-axis amplitude drops. It is feasible to analyze in terms of the off-axis distance (r) and the radius of the Gaussian beam (ω) in each surface the intensity.

$$I(z=0) = I_0 e^{-\frac{2r^2}{\omega^2(z)}} \tag{2}$$

In the simulation, the phase is assumed constant at origin. For a Gaussian beam, the full width of the beam at half of its maximum intensity is defined by:

$$\text{FWHM} = \sqrt{2 \cdot \ln 2}\omega \tag{3}$$

In preliminary analysis, the percentage of power intercepted by apertures, spillover efficiency, is evaluated by truncation analysis as it leads to power loss quantification. By default, far field domain is used (Fraunhofer diffraction), but when this approximation cannot be solved it is necessary to use the second order expansion (Fresnel diffraction). The results obtained are summarized in Fig. 3. There could be losses of up to 10% when the collimator system is defined using only $L1$ and excluding $L2$. The numerical aperture and the far field condition continue to determine the diameter of the beam at the exit of $L1$. Analysis of propagation shows that the use of the $L2$ lens becomes relevant in off-axis fields. The off-axis fields show an energy that varies as a function of the field between 63 and 66% after the cryostat window when $L2$ is incorporated to the design. Gaussian analysis concludes that cryostat window is a critical element in terms of spillover efficiency and truncation of the beams.

2.3 Filters

A set of infrareds—blocking and low pass metal-mesh filters from QMC Instruments Ltd minimizes the thermal loading and the unwanted radiation on the detectors. The 300 K cryostat access consists of an anti-reflection coated HDPE window and a thermal filter. The first radiation shield at 60 K includes two thermal filters. The 4 K and 1 K shields contain an extra infrared thermal filter and a low

	#	Surface	Energy Fraction (after surface)
Collimator Optics	L1	3	0,948
		4	0,946
	L2	6	0,832
		7	0,830
	L3	9	0,656
		10	0,650
Collector Optics	L4	12	0,583
		13	0,578
	L5	14	0,573
		15	0,572

Fig. 3 Results of the Gaussian analysis for each surface. It is shown the energy fraction after each surface. Note the drop of energy between the collimator and the collector optics, due to the cryostat internal window. Filters were not included

pass filter with cut-off frequencies of 12 cm^{-1} and 3.7 cm^{-1}, respectively. Finally, a W-band band pass filter is included in the mK stage for KIDs characterization.

2.4 Collector Optical Design

Collector optics is made up of three conical lenses ($L3$, $L4$ and $L5$) (Fig. 2, including relevant parameters) with an optical path of 160 mm and an $f/0.9$ in the image space (Fig. 2). A cold field stop is incorporated between lenses $L3$ and $L4$ to avoid spurious radiation that could degrade the detector performance and to control straylight. That implies to include an additional optical element ($L5$). An analysis of the diffraction limited performance as well as geometrical light loss effects due to cutting into the diffraction pattern has been developed in order to investigate any significant loss of sensitivity of the optical design.

From the optical point of view, it is desirable to place a field stop in the first focal plane of the collector optics to have an additional element to control the spurious radiation. Telecentricity in the image space plus constraints related to the cryostat dimensions and $f/\#$ variations around $f/1$ defines the design merit function. Simulations defined in the collimator analysis were used for the whole optical design, but, in this case, the aim of the analysis was to evaluate the fraction of the total flux concentrated in one pixel using the EE and the spread of radiation in the focal plane evaluating the PSF. Figure 4 *Left* shows the EE in a single pixel; in our case, an EE higher than 50% is used as internal requirement in the optimization process. Figure 3 *Right* shows the PSF in 2D; the Strehl ratio is calculated by computing the diffraction (PSF) considering aberrations. In this case, ray-tracing simulations show that the Strehl ratio remains above 0.98 even for off-axis fields for the reference frequency of 92.5 GHz.

A preliminary tolerance analysis has been developed. Mounting errors are negligible since assembling structures have been integrated into the optical elements. Nevertheless, this could provide additional paths for unwanted light through the module, being particularly vulnerable to stray light. The RMS tolerance analysis carried out considers the use of $L1$ as a compensator with a compensation range of $\pm$ 1.1 mm.

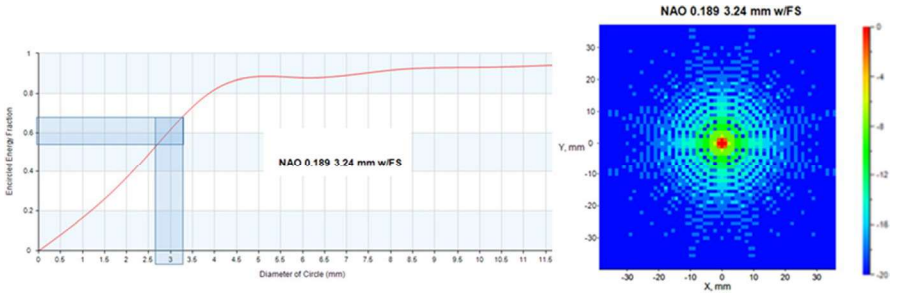

Fig. 4 EE diagram (left), diffraction intensity spread function in dB (right). EE simulations show around 50% of energy over one pixel (blue square) in the focal *plane* (Color figure online)

3 Conclusion

An optical design for KIDs cryogenic optical performance characterization in the W-band is presented. Next steps include the integration of the testbed and evaluation of the incidence beams in the detector, analyzing the impact of different points of interest in the evaluation of KIDs such as, angles of incidence vs radiation, use of horns and telecentricity requirement.

Acknowledgements This work was supported by Spanish Ministry of Science, Innovation and Universities under Grants PID2019-105552RB-C41, MADE (PID2019-105552RB-C44) and PID2019-110610RB-C22. It was also supported by Comunidad de Madrid under Grant P2018/NMT-4291. IMDEA-Nanoscience acknowledges financial support from "Severo Ochoa" Programme for Centers of Excellence in R&D (MINECO, Grant SEV-2016-0686). D.G. and A.G also acknowledge Grant DEFROST N62909-19-1-2053 from ONR Global.

References

1. G. Ulbricht et al., Applications for microwave kinetic induction detectors in advanced instrumentation. Appl. Sci. **11**, 2671 (2021). https://doi.org/10.3390/app11062671
2. S. Shigyuky et al., Development of compact cold optics for millimiter and submillimter wave observation. IEEE Trans. Terahertz Sci. Technol. **5**(1), 49–56 (2015). https://doi.org/10.1109/TTHZ.2014.2367245
3. R. Adam et al., The NIKA2 large-field-of-view millimetre continuum camera for the 30 m IRAM telescope. A&A **609**, A115 (2018)
4. P. Goldsmith, *Quasioptical Systems* (IEEE Press, Piscataway, 1998). https://doi.org/10.1109/9780470546291
5. B. Aja et al., Bi-layer kinetic inductance detectors for W-band. IEEE/MTT-S Int. Microw. Symp (IMS) **2020**, 932–935 (2020). https://doi.org/10.1109/IMS30576.2020.9223828